

## Short communication

Graphene-based contrast agents for photoacoustic and thermoacoustic tomography<sup>☆</sup>Gaurav Lalwani<sup>a,1</sup>, Xin Cai<sup>b,1</sup>, Liming Nie<sup>b</sup>, Lihong V. Wang<sup>b,2,\*</sup>, Balaji Sitharaman<sup>a,3,\*\*</sup><sup>a</sup> Department of Biomedical Engineering, Stony Brook University, Stony Brook, NY 11794-5281, USA<sup>b</sup> Optical Imaging Laboratory, Department of Biomedical Engineering, Washington University in St. Louis, Campus Box 1097, One Brookings Drive, St. Louis, MO 63130, USA

## ARTICLE INFO

## Article history:

Received 14 July 2013

Received in revised form 18 September 2013

Accepted 8 October 2013

## Keywords:

Graphene

Photoacoustic tomography

Thermoacoustic tomography

Contrast agents

Microwave imaging

## ABSTRACT

In this work, graphene nanoribbons and nanoplatelets were investigated as contrast agents for photoacoustic and thermoacoustic tomography (PAT and TAT). We show that oxidized single- and multi-walled graphene oxide nanoribbons (O-SWGNRs, O-MWGNRs) exhibit approximately 5–10 fold signal enhancement for PAT in comparison to blood at the wavelength of 755 nm, and approximately 10–28% signal enhancement for TAT in comparison to deionized (DI) water at 3 GHz. Oxidized graphite microparticles (O-GMPs) and exfoliated graphene oxide nanoplatelets (O-GNPs) show no significant signal enhancement for PAT, and approximately 12–29% signal enhancement for TAT. These results indicate that O-GNRs show promise as multi-modal PAT and TAT contrast agents, and that O-GNPs are suitable contrast agents for TAT.

© 2013 The Authors. Published by Elsevier GmbH. All rights reserved.

## 1. Introduction

Hybrid imaging modalities, such as photoacoustic (PA) tomography (PAT) [1] and thermoacoustic (TA) tomography (TAT) [2], have been developed for different applications. PAT/TAT combines advantages of pure ultrasound and pure optical imaging/radio frequency (rf), providing good spatial resolution, great penetration depth, and high soft-tissue contrast. These imaging modalities are based on detection of acoustic waves from an object that absorbs electromagnetic (EM) energy (laser in PAT and microwave in TAT). Endogenous molecules, such as hemoglobin, melanin, and water/ion, can absorb EM energy, producing acoustic waves. High resolution PAT and/or TAT enable functional brain imaging [3],

breast cancer detection [4], melanoma detection [5], tumor angiogenesis [6], and functional molecular imaging [2]. However, in cases when endogenous molecules are insufficient, exogenous contrast agents (CAs) are developed and administered. Contrast-enhanced PAT has been applied in lymph node mapping [7], multiscale imaging of tissue engineering scaffolds [8,9], and molecular, cellular, and functional imaging [10,11]. A variety of CAs for PAT have been reported, such as, carbon nanoparticles [7,12–14], metallic nanoparticles [11,15–17], and organic dyes [18]. In comparison to PAT, fewer reports have focused on development of CAs for TAT. Superparamagnetic iron oxide nanoparticles, single- and multi-walled carbon nanotubes (SWCNT and MWCNT), and air-filled microbubbles have been investigated as CAs for TAT [2,13,19,20].

In this work, we investigate efficacy of graphene nanoparticles, prepared by two widely used methods ((1): longitudinal unzipping method [21], (2): modified Hummer's method of oxidation [22]) as CAs for PAT and TAT. We compare PA and TA signal amplitudes of oxidized single- and multi-walled graphene oxide nanoribbons (O-SWGNRs and O-MWGNRs), and oxidized graphene nanoplatelets (O-GNPs) to pristine SWCNTs, pristine MWCNTs, pristine graphite microparticles (GMPs), and oxidized graphite microparticles (O-GMP).

## 2. Results and discussions

O-SWGNRs, O-MWGNRs, and O-GNPs were synthesized as reported previously [22,23]. Pristine SWCNTs, MWCNTs, and GMPs

<sup>☆</sup> This is an open-access article distributed under the terms of the Creative Commons Attribution-NonCommercial-No Derivative Works License, which permits non-commercial use, distribution, and reproduction in any medium, provided the original author and source are credited.

\* Corresponding author at: Department of Biomedical Engineering, Washington University in St. Louis, Campus Box 1097, One Brookings Drive, St. Louis, MO 63130, USA.

\*\* Corresponding author at: Department of Biomedical Engineering, Bioengineering Building Room 115, Stony Brook University, Stony Brook, NY 11794-5281, USA. Tel.: +1 631 632 1810; fax: +1 631 632 8577.

E-mail addresses: [lhwang@seas.wustl.edu](mailto:lhwang@seas.wustl.edu) (L.V. Wang),

[balaji.sitharaman@stonybrook.edu](mailto:balaji.sitharaman@stonybrook.edu), [balajisitharaman@yahoo.com](mailto:balajisitharaman@yahoo.com) (B. Sitharaman).

<sup>1</sup> These authors contributed equally to the work.

<sup>2</sup> PAT and TAT.

<sup>3</sup> Graphene contrast agents.

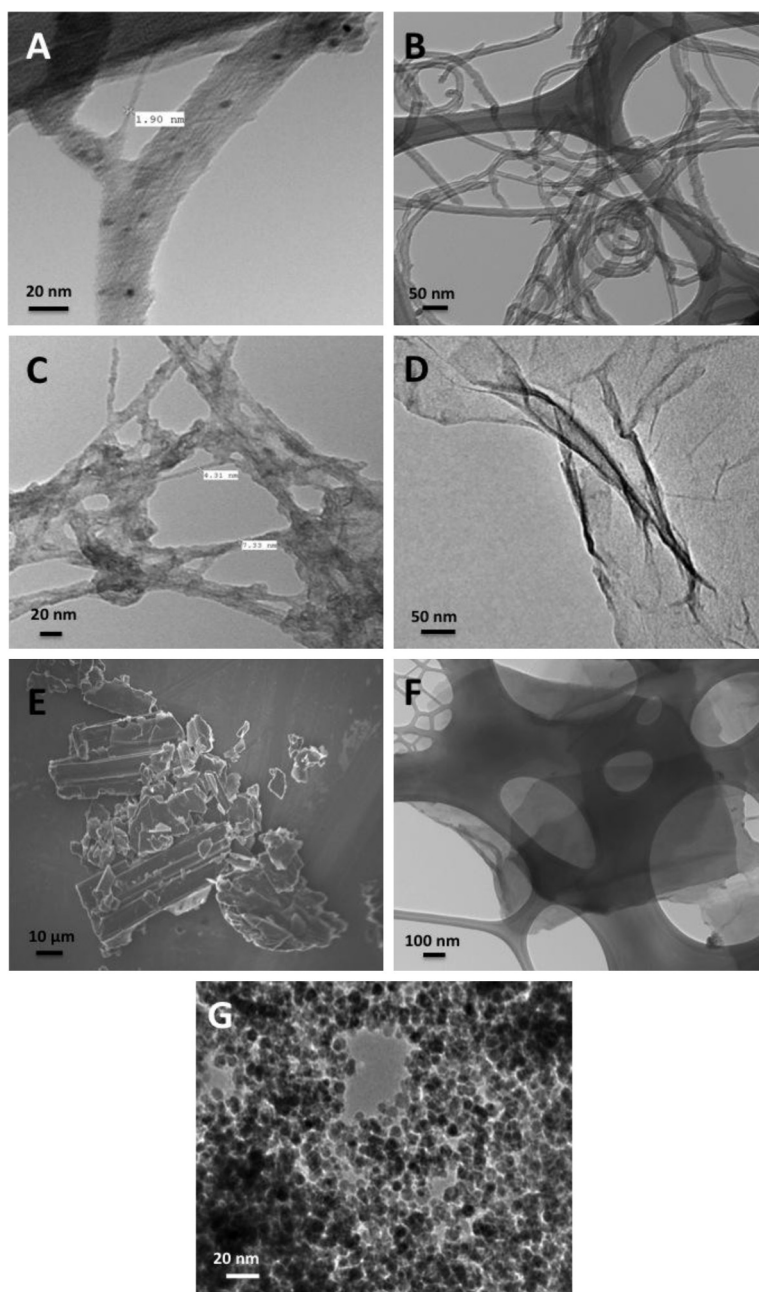


**Fig. 1.** Representative transmission electron microscopy images of (A) single-walled carbon nanotubes (SWCNTs), (B) multi-walled carbon nanotubes (MWCNTs), (C) oxidized single-walled graphene nanoribbons (O-SWGNRs), (D) oxidized multi-walled graphene nanoribbons (O-MWGNRs), (F) oxidized graphite microparticles (O-GMP), and (G) exfoliated graphene nanoplatelets (O-GNP). Image (E) is a scanning electron micrograph of pristine GMPs.

were used as starting materials in the preparation of O-SWGNRs, O-MWGNRs, and O-GNPs, respectively. O-GMPs are intermediate product formed during the synthesis of O-GNPs. These nanomaterials were characterized by Raman spectroscopy and electron microscopy (EM). Raman spectroscopic characterization of SWCNTs, MWCNTs, O-SWGNRs, O-MWGNRs, GMPs, O-GMPs, and O-GNPs has been reported previously [22,24–26]. Table 1 lists the size distribution of various nanomaterials. Fig. 1 shows representative transmission EM (TEM) images of all nanomaterials used in the study (scanning EM (SEM) for GMPs). SWCNTs (Fig. 1A) and MWCNTs (Fig. 1B) were nanotubes of lengths  $\approx 3$ – $30 \mu\text{m}$  and  $0.5$ – $200 \mu\text{m}$ , and diameters  $\approx 1$ – $2 \text{ nm}$  and  $\approx 20$ – $30 \text{ nm}$ , respectively. O-SWGNRs (Fig. 1C) and O-MWGNRs (Fig. 1D) possessed lengths  $\approx 0.5$ – $1 \mu\text{m}$  and  $0.5$ – $1.5 \mu\text{m}$ , and diameters of  $\approx 3$ – $6 \text{ nm}$

and  $\approx 60$ – $90 \text{ nm}$ , respectively, confirming complete unzipping of SWCNTs and MWCNTs ( $\pi^*$  diameter). Pristine GMPs were  $< 45 \mu\text{m}$  in size (Fig. 1E). O-GMPs (Fig. 1F) were loosely arranged sheets of a few layered graphene ( $\approx 8$  sheets, size  $> 1 \mu\text{m}$ ) whereas O-GNPs (Fig. 1G) had  $\approx 2$ – $4$  graphene sheets and diameters of  $\approx 5$ – $15 \text{ nm}$ .

We have estimated that future *in vivo* preclinical safety (acute toxicity) studies to establish the therapeutic dosages of graphene would require their administration at a range of dosages; from  $50 \text{ mg/kg}$  upto possibly  $\geq 500 \text{ mg/kg}$  body weight of the small animal [27]. If the graphene formulations are injected at a dose of  $50$  or  $500 \text{ mg/kg}$  body weight of a  $250 \text{ g}$  rat (total circulating blood volume  $12$ – $13 \text{ ml}$ ), its steady state blood concentration after the first pass would be  $\sim 1$  or  $10 \text{ mg/ml}$ , respectively. Thus, a median concentration of  $5 \text{ mg/ml}$  was chosen for this study. Since

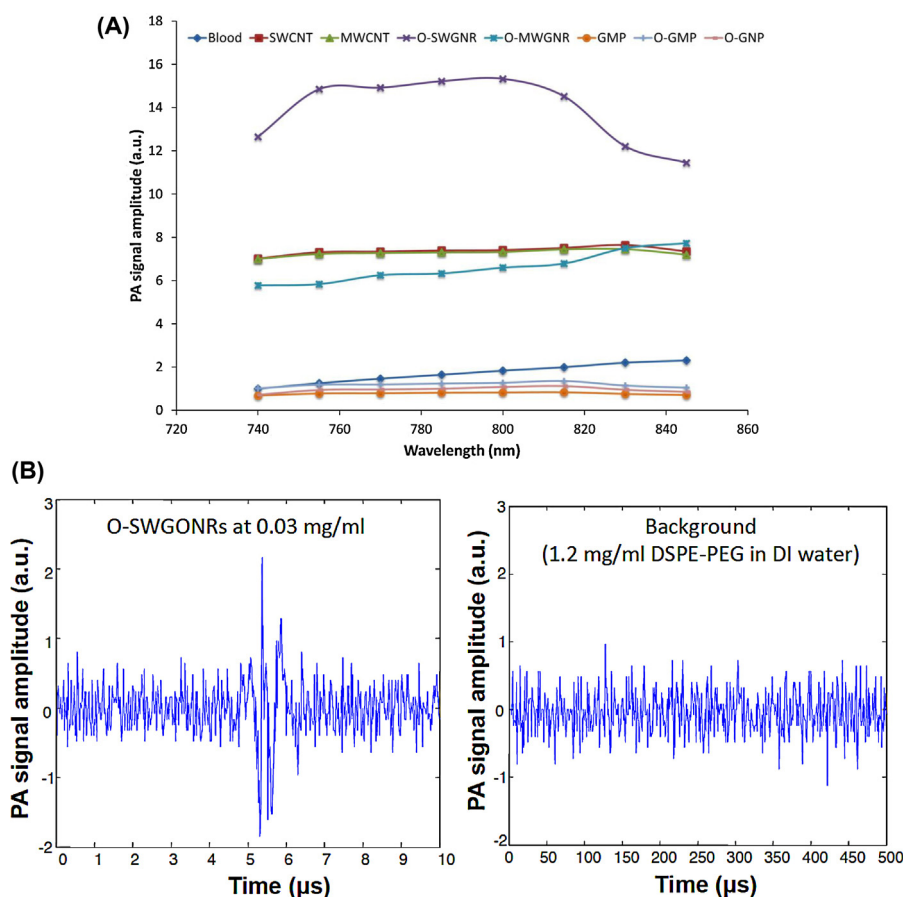


**Fig. 2.** (A) Photoacoustic spectral amplitudes of blood, single-walled carbon nanotubes (SWCNTs), multi-walled carbon nanotubes (MWCNTs), oxidized single-walled graphene nanoribbons (O-SWGNRs), oxidized multi-walled graphene nanoribbons (O-MWGNRs), micro-graphite flakes (GMPs), oxidized graphite microparticles (O-GMPs), and exfoliated graphene nanoplatelets (O-GNPs). PA signal amplitudes are normalized to that of blood at 740 nm. (B) PA signal amplitude of O-SWGNRs at 0.03 mg/ml concentration compared to background (1.2 mg/ml of DSPE-PEG solution).

hemoglobin is a dominant optical absorber producing strong PA signal in human tissue, efficacy of these nanomaterials was compared with blood in the NIR wavelength window. Fig. 2A shows PA signal amplitudes obtained from a tygon tube (I.D. 250  $\mu\text{m}$ , O.D. 500  $\mu\text{m}$ ) filled with SWCNT, MWCNT, O-SWGNR, O-MWGNR, micro-graphite flakes, O-GMP, O-GNP and lysed bovine blood (905–250, Quad Five), respectively. The signals were normalized to that for blood at 740 nm. At 755 nm excitation wavelength, peak-to-peak PA signal amplitudes obtained from micro-graphite flakes, O-GMPs, and O-GNPs were comparable to that from blood alone. In contrast, those from SWCNTs, MWCNTs, O-SWGNRs and O-MWGNRs were more than 5 times stronger than that from blood, in which, O-SWGNRs showed  $\sim 14$  times stronger signal. At 5 mg/ml concentration, PA signal intensities obtained from gold nanoparticles were 3 times greater, and methylene blue dye were similar, compared to blood [28,29]. We detected a very high signal-to-noise ratio (SNR; ratio of the average signal to the

standard deviation of the background) of O-SWGNRs at 5 mg/ml. The SNR was  $>170$  and suggested that the concentration of the O-SWGNRs can be as low as 0.03 mg/ml using PAT. At this low O-SWGNR concentration, a 2-fold increase in PA signal was measured compared to background (1.2 mg/ml DSPE-PEG in DI water) (Fig. 2B). These results suggest that minimum detectable concentration of O-SWGNRs will be comparable to other PA contrast agents such as gold nanoparticles [17,30]. Furthermore, the results showed that PA signal obtained from these nanomaterials exceeded inherent blood signal over the investigated NIR bandwidth, suggesting their utility for *in vivo* imaging.

Water and ions are two well-known sources of microwave absorbers in human tissue, and they generate strong TA signals. Therefore, to show that nanomaterials can function as CAs for TAT, we compared TA signal of nanomaterials to that of DI water. Fig. 3B shows TA signals obtained from a low-density polyethylene (LDPE) vial (I.D. = 6 mm and 1.5 cc volume) filled with DI water, SWCNTs,

**Table 1**  
Size distribution of various nanomaterials.

Nanomaterial	Length	Diameter
Single-walled carbon nanotubes (SWCNTs)	3–30 $\mu\text{m}$	1–2 nm
Multi-walled carbon nanotubes (MWCNTs)	0.5–200 $\mu\text{m}$	20–30 nm
Oxidized single-walled graphene nanoribbons (O-SWGNRs)	0.5–1 $\mu\text{m}$	3–6 nm
Oxidized multi-walled graphene nanoribbons (O-MWGNRs)	0.5–1.5 $\mu\text{m}$	60–90 nm
Pristine graphite microparticles (GMPs)	–	$<45 \mu\text{m}$
Oxidized graphite microparticles (O-GMPs)	–	$>1 \mu\text{m}$
Oxidized graphene nanoplatelets (O-GNP)	–	5–15 nm

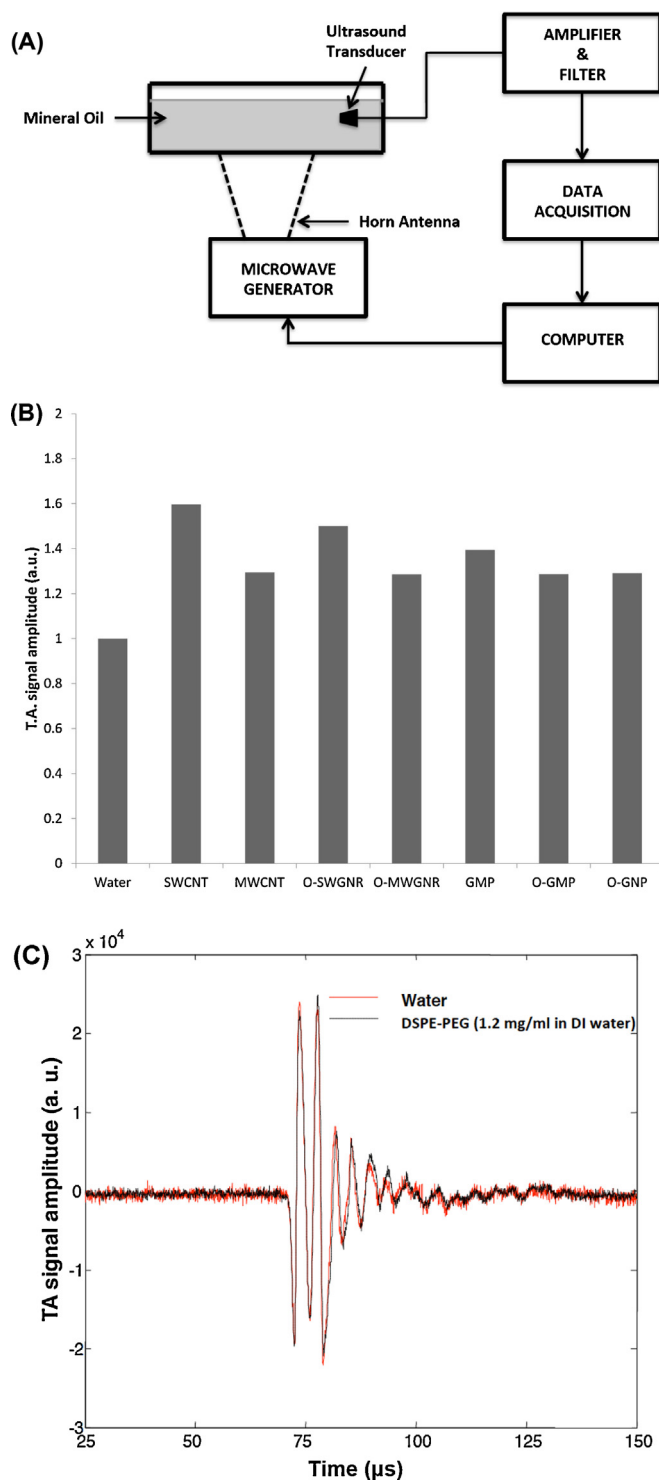


**Fig. 3.** (A) Schematic depiction of the experimental setup for thermoacoustic signal measurements. (B) Thermoacoustic signal amplitudes of water, single-walled carbon nanotubes (SWCNTs), multi-walled carbon nanotubes (MWCNTs), oxidized single-walled graphene nanoribbons (O-SWGNRs), oxidized multi-walled graphene nanoribbons (O-MWGNRs), micro-graphite flakes (GMPs), oxidized graphite microparticles (O-GMP), and exfoliated graphene nanoplatelets (O-GNP) at 3 GHz. TA signals are normalized to that of water at 3 GHz. (C) TA signal amplitude of DSPE-PEG compared to DI water.

MWCNTs, O-SWGNRs, O-MWGNRs, GMPs, O-GMPs, and O-GNPs, respectively. The signal amplitudes were normalized to DI water. Additionally, TA signal amplitude of DSPE-PEG was comparable to DI water (Fig. 3C), and LDPE vial does not generate any measurable TA signal [13]. At 3 GHz, the SNR of the nanomaterials was  $>170$ , and the nanomaterials exhibited  $\approx 10$ –28% TA signal enhancement compared to DI water.

To the best of our knowledge, this is the first study exploring and comparing efficacy of graphene nanoparticles prepared via longitudinal “unzipping” method and Hummer’s method as CAs for multimodal PAT and TAT. These results indicate that O-GNPs could be used for multimodal PAT and TAT applications, and O-GNPs are suitable CAs for TAT. Bulk of the work performed towards developing CAs for PAT has been focused on metallic nanoparticles,

organic dye molecules, and carbon nanotubes. In comparison to those CAs, graphene possesses several benefits: (1) Compared to carbon nanotubes, graphene possesses larger surface area, lower aspect ratio, and better dispersibility in most biological media. These properties are important, for most *in vivo* applications. Furthermore, colloidal dispersions (with high stability and less aggregation) of graphene sheets can be achieved without impurities that may be harmful in biological systems [31,32]. (2) The  $sp^2$  bonded carbon sheets of graphene can be directly functionalized for targeting and drug delivery [33]. For other PAT/TAT CAs, such as gold nanoparticles and organic dye molecules, to disperse and stabilize gold nanoparticles in solution or embed organic dye molecules, functionalization is performed on the biocompatible coating/capping agent. (3) O-GNPs and O-GNRs have been reported as CAs for other whole-body imaging applications such as magnetic resonance imaging [22] and nuclear imaging [34]. Therefore, they can be developed as multimodal CAs that provide complementary information at micro- to macroscopic length scales. (4) Graphene can be developed as therapeutic (simultaneous therapy and diagnostics) agent combining PAT/TAT molecular imaging and NIR-induced hyperthermia [33]. Due to these unique features, graphene may serve as a platform for the design of multi-modal imaging and multi-therapeutic approaches. Indeed, several *in vitro* and *in vivo* safety and efficacy studies on these graphene nanoparticles have been reported for various biomedical applications [23,35].

### 3. Materials and methods

#### 3.1. Synthesis and characterization of nanomaterials

SWCNTs (Cheap Tubes Inc., VT, USA) and MWCNTs (Sigma Aldrich, NY, USA) were used as received. O-SWGNRs, O-MWGNRs, O-GMPs, and O-GNPs were synthesized and characterized as reported previously [22–24]. All nanomaterials were dispersed at 5 mg/ml in DSPE-PEG for PA and TA measurements.

#### 3.2. Photoacoustic (PA) imaging

A deep reflection-mode PA imaging system was used (Scheme 1 in Ref. [36]) for PA tests of graphene samples. A tunable Ti:sapphire laser (LT-2211A; Lotis TII, Minsk, Belarus) pumped by a Q-switched Nd:YAG (LS-2137; Lotis TII) laser was used for PA excitation (pulse width: 5 ns, pulse repetition rate: 10 Hz). A 5-MHz central frequency, spherically focused ultrasonic transducer (V308; Panametrics-NDT, Waltham, MA, USA), low-noise amplifier (5072PR; Panametrics-NDT), a digital oscilloscope (TDS 5054; Tektronix, Beaverton, OR, USA) were used to acquire, amplify, and record signals. The reported PA signal amplitudes have been normalized for laser fluence at their corresponding wavelengths.

#### 3.3. Thermoacoustic (TA) imaging

Fig. 3A is a schematic depiction of the experimental setup for TA measurements. TA results were obtained from a TAT system with a 3.0-GHz microwave generator (pulse width = 0.6  $\mu$ s, repetition rate = 10 Hz) and a 20 dB amplifier. The pulses (average power density = 4.5 mW/cm<sup>2</sup>, within safety standard) were guided toward the target through a horn antenna (11 cm  $\times$  7 cm) [37]. A 1-MHz spherically focused transducer with a bandwidth of 70% (V314, Panametrics, Olympus) was used to receive TA signals from samples placed in a plastic tank filled with mineral oil for ultrasound coupling. The received TA signals were amplified and stored by a data-acquisition (DAQ) card (CS 14200; Gage Applied, IL) [38]. The microwave generator simultaneously triggered data acquisition.

### Conflict of interest statement

The authors declare no conflict of interest.

### Acknowledgments

We are grateful to Sandra Matteucci for proof reading of the manuscript. Our work was sponsored by NIH Director's New Innovator Award 1DP2OD007394-01 (to S.B.), Wallace H. Coulter Foundation (S.B.), and NIH grants R01 EB008085, R01 CA140220, R01 CA157277, R01 CA159959, U54 CA136398, and DP1 EB016986 – NIH Director's Pioneer Award (to L.V.W.). L.V.W. has a financial interest in Microphotoacoustics, Inc. and Endra, Inc., which, however, did not support this work.

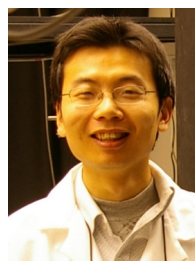
### References

- [1] Wang LV. Multiscale photoacoustic microscopy and computed tomography. *Nat Photon* 2009;3:503–9.
- [2] Nie L, Ou Z, Yang S, Xing D. Thermoacoustic molecular tomography with magnetic nanoparticle contrast agents for targeted tumor detection. *Med Phys* 2010;37:4193–200.
- [3] Wang X, Pang Y, Ku G, Xie X, Stoica G, Wang LV. Noninvasive laser-induced photoacoustic tomography for structural and functional *in vivo* imaging of the brain. *Nat Biotechnol* 2003;21:803–6.
- [4] Ermilov SA, Khamapirad T, Conjusteau A, Leonard MH, Laceywell R, Mehta K, et al. Laser photoacoustic imaging system for detection of breast cancer. *J Biomed Opt* 2009;14:024007.
- [5] Zhang HF, Maslov K, Stoica G, Wang LV. Functional photoacoustic microscopy for high-resolution and noninvasive *in vivo* imaging. *Nat Biotechnol* 2006;24:848–51.
- [6] Siphanto RI, Thumma KK, Kolkman RG, van Leeuwen TG, de Mul FF, van Neck JW, et al. Serial noninvasive photoacoustic imaging of neovascularization in tumor angiogenesis. *Opt Express* 2005;13:89–95.
- [7] De la Zerd A, Zavaleta C, Keren S, Vaithilingam S, Bodapati S, Liu Z, et al. Carbon nanotubes as photoacoustic molecular imaging agents in living mice. *Nat Nanotechnol* 2008;3:557–62.
- [8] Cai X, Paratata BS, Hu S, Sitharaman B, Wang LV. Multiscale photoacoustic microscopy of single-walled carbon nanotube-incorporated tissue engineering scaffolds. *Tissue Eng C Methods* 2012;18:310–7.
- [9] Avti PK, Hu S, Favazza C, Mikos AG, Jansen JA, Shroyer KR, et al. Detection, mapping, and quantification of single walled carbon nanotubes in histological specimens with photoacoustic microscopy. *PLoS One* 2012;7:e35064.
- [10] Mallidi S, Larson T, Aaron J, Sokolov K, Emelianov S. Molecular specific photoacoustic imaging with plasmonic nanoparticles. *Opt Express* 2007;15:6583–8.
- [11] Agarwal A, Huang SW, O'Donnell M, Day KC, Day M, Kotov N, et al. Targeted gold nanorod contrast agent for prostate cancer detection by photoacoustic imaging. *J Appl Phys* 2007;102:064701–64704.
- [12] Pramanik M, Song KH, Swierczewska M, Green D, Sitharaman B, Wang LV. *In vivo* carbon nanotube-enhanced non-invasive photoacoustic mapping of the sentinel lymph node. *Phys Med Biol* 2009;54:3291–301.
- [13] Pramanik M, Swierczewska M, Green D, Sitharaman B, Wang LV. Single-walled carbon nanotubes as a multimodal-thermoacoustic and photoacoustic-contrast agent. *J Biomed Opt* 2009;14:034018.
- [14] Wu L, Cai X, Nelson K, Xing W, Xia J, Zhang R, et al. A green synthesis of carbon nanoparticles from honey and their use in real-time photoacoustic imaging. *Nano Res* 2013;1–14.
- [15] Pan D, Cai X, Yalaz C, Senpan A, Omanakuttan K, Wickline SA, et al. Photoacoustic sentinel lymph node imaging with self-assembled copper neodecanoate nanoparticles. *ACS Nano* 2012;6:1260–7.
- [16] Cai X, Li W, Kim CH, Yuan Y, Wang LV, Xia Y. *In vivo* quantitative evaluation of the transport kinetics of gold nanocages in a lymphatic system by noninvasive photoacoustic tomography. *ACS Nano* 2011;5:9658–67.
- [17] Pan D, Pramanik M, Senpan A, Yang X, Song KH, Scott MJ, et al. Molecular photoacoustic tomography with colloidal nanobeacons. *Angew Chem* 2009;48:4170–3.
- [18] Kim G, Huang SW, Day KC, O'Donnell M, Agayan RR, Day MA, et al. Indocyanine-green-embedded PEBBLES as a contrast agent for photoacoustic imaging. *J Biomed Opt* 2007;12:044020.
- [19] Jin X, Keho A, Meissner K, Wang LV. Iron-oxide nanoparticles as a contrast agent in thermoacoustic tomography. *Proc SPIE* 2007;6437.
- [20] Mashal A, Booske JH, Hagness SC. Toward contrast-enhanced microwave-induced thermoacoustic imaging of breast cancer: an experimental study of the effects of microbubbles on simple thermoacoustic targets. *Phys Med Biol* 2009;54:641–50.
- [21] Kosynkin DV, Higginbotham AL, Sinititskii A, Lomeda JR, Dimiev A, Price BK, et al. Longitudinal unzipping of carbon nanotubes to form graphene nanoribbons. *Nature* 2009;458:872–6.

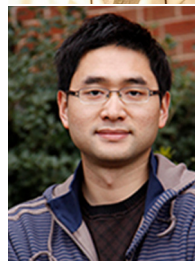
- [22] Paratala BS, Jacobson BD, Kanakia S, Francis LD, Sitharaman B. Physicochemical characterization, and relaxometry studies of micro-graphite oxide, graphene nanoplatelets, and nanoribbons. *PLoS One* 2012;7:e38185.
- [23] Mullick Chowdhury S, Lalwani G, Zhang K, Yang JY, Neville K, Sitharaman B. Cell specific cytotoxicity and uptake of graphene nanoribbons. *Biomaterials* 2013;34:283–93.
- [24] Lalwani G, Henslee AM, Farshid B, Lin L, Kasper FK, Qin Y-X, et al. Two-dimensional nanostructure-reinforced biodegradable polymeric nanocomposites for bone tissue engineering. *Biomacromolecules* 2013;14:900–9.
- [25] Lalwani G, Kwaczala AT, Kanakia S, Patel SC, Judex S, Sitharaman B. Fabrication and characterization of three-dimensional macroscopic all-carbon scaffolds. *Carbon* 2013;53:90–100.
- [26] Lalwani G, Henslee AM, Farshid B, Parmar P, Lin L, Qin YX, et al. Tungsten disulfide nanotubes reinforced biodegradable polymers for bone tissue engineering. *Acta Biomater* 2013;9:8365–73.
- [27] Kanakia S, Toussaint J, Mullick Chowdhury S, Lalwani G, Tembulkar T, Button T, et al. Physicochemical characterization of a novel graphene-based magnetic resonance imaging contrast agent. *Int J Nanomed* 2013;8:2821–33.
- [28] Pan D, Pramanik M, Senpan A, Ghosh S, Wickline SA, Wang LV, et al. Near infrared photoacoustic detection of sentinel lymph nodes with gold nanobeacons. *Biomaterials* 2010;31:4088–93.
- [29] Song KH, Stein EW, Margenthaler JA, Wang LV. Noninvasive photoacoustic identification of sentinel lymph nodes containing methylene blue in vivo in a rat model. *J Biomed Opt* 2008;13:054033.
- [30] Eghtedari M, Oraevsky A, Copland JA, Kotov NA, Conjusteau A, Motamedi M. High sensitivity of in vivo detection of gold nanorods using a laser optoacoustic imaging system. *Nano Lett* 2007;7:1914–8.
- [31] Mao HY, Laurent S, Chen W, Akhavan O, Imani M, Ashkarran AA, et al. Graphene: promises, facts, opportunities, and challenges in nanomedicine. *Chem Rev* 2013;113:3407–24.
- [32] Bussy C, Ali-Boucetta H, Kostarelos K. Safety considerations for graphene: lessons learnt from carbon nanotubes. *Accounts Chem Res* 2013;46(3):692–701.
- [33] Huang P, Xu C, Lin J, Wang C, Wang X, Zhang C, et al. Folic acid-conjugated graphene oxide loaded with photosensitizers for targeting photodynamic therapy. *Theranostics* 2011;1:240–50.
- [34] Cornelissen B, Able S, Kersemans V, Waghorn PA, Myhra S, Jurkshat K, et al. Nanographene oxide-based radioimmunoconstructs for in vivo targeting and SPECT imaging of HER2-positive tumors. *Biomaterials* 2013;34:1146–54.
- [35] Shen H, Zhang L, Liu M, Zhang Z. Biomedical applications of graphene. *Theranostics* 2012;2:283–94.
- [36] Song KH, Wang LV. Deep reflection-mode photoacoustic imaging of biological tissue. *J Biomed Opt* 2007;12:060503.
- [37] (SCC39) IICoES. IEEE Standard for Safety Levels with Respect to Human Exposure to Radio Frequency Electromagnetic Fields, 3 kHz–300 GHz. IEEE Std C951-2005 (Revision of IEEE Std C951-1991); 2006;p. 1–238.
- [38] Nie L, Guo Z, Wang LV. Photoacoustic tomography of monkey brain using virtual point ultrasonic transducers. *J Biomed Opt* 2011;16:076005.



Gaurav Lalwani received his B.Tech. in Biotechnology from SRM University, Chennai, India, in 2010, and M.S. in Biomedical Engineering from Stony Brook University, New York, in 2012. He is currently working towards a Ph.D. in Biomedical Engineering at Stony Brook University under the guidance of Dr. Balaji Sitharaman. His research areas include biomaterials and regenerative medicine. He is working on the design of nanoparticle-reinforced biodegradable polymeric nanocomposites and multi-functional three-dimensional macroscopic all-carbon scaffolds for tissue engineering applications, and graphene-based nanostructures as multimodal contrast agents for medical diagnostics.



Xin Cai earned his M.S. degree at Huazhong University of Science and Technology, Wuhan, China, in 2008. He is currently a research associate in the Optical Imaging Laboratory, Department of Biomedical Engineering, Washington University in St. Louis. His research interests are the developments of non-ionizing and non-invasive novel biomedical imaging techniques, including photoacoustic imaging, fluorescence imaging, and ultrasonic imaging. He has published 22 papers in peer-reviewed journals.



Dr. Liming Nie earned his B.S. in 2005 and Ph.D. in 2010, both in Optics, from South China Normal University. His Ph.D. project was focused on microwave-induced thermoacoustic tomography and its biomedical application. In August 2010, he joined Optical Imaging Lab at Washington University in St. Louis under the mentorship of Dr. Lihong V. Wang. His project involved noninvasive photoacoustic imaging of the primate brain and reconstruction correction for imaging distortion. In October 2012, he joined Dr. Shawn Chen's Laboratory of Molecular and Nanomedicine (LOMIN), NIBIB, NIH. His current research is focused on developing photoacoustic/ultrasound imaging system, image processing, and molecular therapeutics.



Lihong V. Wang earned his Ph.D. degree at Rice University, Houston, Texas under the tutelage of Robert Curl, Richard Smalley, and Frank Tittel. He is Gene Beare Distinguished Professor at Washington Univ. His laboratory invented functional photoacoustic tomography, 3D photoacoustic microscopy, and time-reversed ultrasonically encoded (TRUE) optical focusing. He has published 342 journal articles and delivered 357 invited talks. His Google Scholar h-index and citations have reached 80 and 25,500, respectively. He has received 34 grants as PI with a budget of \$41M. He is the Editor-in-Chief of the *Journal of Biomedical Optics*. He co-founded two companies to commercialize photoacoustic tomography. He is a Fellow of the AIMBE, OSA, IEEE, and SPIE. His book entitled "Biomedical Optics: Principles and Imaging" won the Goodman Award. He was awarded OSA's C.E.K. Mees Medal and IEEE's Technical Achievement Award for "seminal contributions to photoacoustic tomography and Monte Carlo modeling of photon transport in biological tissues and for leadership in the international biophotonics community".



Balaji Sitharaman is an Assistant Professor of Biomedical Engineering at Stony Brook University. He received his B.S. (2000) from the Indian Institute of Technology at Kharagpur. He received his M.A and Ph.D. (2005) from Rice University, where he also completed his postdoctoral research (2005–2007) as the J. Evan Attwell-Welch Postdoctoral Fellow at the Richard E. Smalley Institute for Nanoscale Science and Technology. Sitharaman's research program is at the interface of nanotechnology, regenerative and molecular medicine and synergizes the advancements in each of these fields to tackle problems related to diagnosis/treatment of disease and tissue regeneration. He is the author of over 40 peer-reviewed publications. He has received several awards for his research including NIH Director's New Innovator Award from the National Institute of Health, the Idea Award from the Department of Defense, the Carol M. Baldwin Breast Cancer Research Award from the Carol Baldwin Foundation and the George Kozmetsky Award from the Nanotechnology Foundation of Texas.